Resonant stretching of cells and other elastic objects from transient cavitation

Tandiono Tandiono,†*[a] Evert Klaseboer, †*[a] Siew-Wan Ohl,[a] Dave Siak-Wei Ow,[b] Andre Boon-Hwa Choo,[b] Fenfang Li[c] and Claus-Dieter Ohl[c]

The phenomenon of stretched cells in the vicinity of an oscillating bubble is investigated in this work. Experiments reveal that a red blood cell can be stretched up to five times its initial size towards the end of the collapse of a laser-induced cavitation bubble. We hypothesize that the cell elasticity is crucial for the elongation. In order to get insight in the physics involved, numerical simulations based on potential flow theory (with the boundary element method) are performed. A simple membrane tension model for the elongating cell is employed. We observe that the stretching can only occur if the cell exhibits some elastic properties within a certain threshold. The maximum elongation occurs when the oscillation of the bubble and cell are out of phase, that is, the bubble oscillates at half the oscillation time of the cell.

1. Introduction

A better understanding of the complex interaction between an oscillating cavitation bubble and an elastic object such as a cell (or emulsion droplet, biomaterial etc.) is becoming more important with the increasing usage of such bubbles in biomedical and industrial applications. Whether the bubbles are created using ultrasound or focused laser pulses, strong shear can be generated upon collapse. In many instances the bubble collapse is non-spherical and high speed jets emerge, especially near boundaries.[1] The induced liquid shear can be used for emulsion generation,[2] ablation, cutting, and disruption of biological tissue,[3,4] lithotripsy,[5,6] dentistry applications such as removal of biofilm in a root-canal[7] and drug delivery into dentinal tubules.[8] For applications involving biological cells, cavitation bubbles have been utilized for the disruption of individual cell membranes,[9] drug delivery and gene transfection.[10-12]

Knowledge of the exact physical interaction between the oscillating bubble and a nearby cell or elastic object is essential to benefit optimally from these techniques. Marmottant and Hilgenfeldt[13] have shown that a single radially oscillating bubble can cause deformation to the membrane of a nearby vesicle. Their study hinted at the underlying mechanisms of sonoporation, where oscillating ultrasonic bubbles could cause the temporary opening of a cell membrane for drug or gene delivery. In another application, Dijkink *et al.*[14] created a laser-induced bubble near to a rigid boundary covered with adherent cancer cells. Using high speed photography, it was shown that some of the cells near the oscillating bubbles were detached and subsequently lysed.

More recently, Tandiono *et al.*[15] developed a customized ultrasonic microfluidic system with a confined geometry to allow for the physical lysis of bacterial and yeast cells. The bacterium *Escherichia coli* and yeast *Pichia pastoris* cells were found to be efficiently lysed in the 20 μm thick microfluidic channel by the oscillating ultrasonic bubbles. While the presence of these bubbles is necessary for cell lysis, it is not clear, how the lysis of the cells is actually accomplished. In this work, we attempt to study in a controlled manner the interaction of an oscillating bubble with a single red blood cell in a similar microfluidic setup using high speed photography and numerical simulations based on a boundary element code. We aim to unravel the physical mechanism involved with typical examples of experiments showing the characteristic stretching behaviours of red blood cells near an oscillating bubble in a microchannel (Section 2), followed by numerical simulations of a bubble near a vesicle with varying membrane tension values. In Section 3, a detailed discussion on the validity of the obtained results will be given prior to the conclusions in Section 4. The importance of the elasticity of the cell, and the distance between a cell and an oscillating bubble for the observed phenomena will be highlighted.

2. An oscillating bubble near an elastic object

2.1 Experimental results: images of a red blood cell near an oscillating bubble

[a] *Institute of High Performance Computing, 1 Fusionopolis Way, #16-16 Connexis, Singapore 138632, Singapore. Fax: (65) 6467 4350; Tel: (65) 6419 1111; Email: evert@ihpc.a-star.edu.sg, tandiono@ihpc.a-star.edu.sg*

[b] *Bioprocessing Technology Institute, 20 Biopolis Way, #06-01 Centros, Singapore 138668, Singapore*

[c] *Division of Physics and Applied Physics, School of Physical and Mathematical Sciences, Nanyang Technological University, Singapore 637371, Singapore*

† These authors contribute equally to this work.

A schematic illustration of the bubble-cell configuration is shown in Fig. 1. In short, human erythrocytes (red blood cells) are introduced into a microchamber, and an oscillating bubble is generated in the vicinity of a cell by localized heating of the liquid sample with a high-intensity laser pulse. The cells are replaced with a fresh batch every half an hour or less. Therefore, although the cells may sit on the bottom surface of the microchamber, it is unlikely that they are attached to the substrate during the experiments. For more details on the experimental setup (Fig. 1*A*) and the procedure of generating the bubble, the reader is referred to Appendix A.

By varying the laser energy, we can control the size of the bubble obtained; in this experiment the maximum radius R_m ranges between 30 and 100 µm. The bubble size is always larger than the cell which has an initial radius of about 4 µm. The effect of the distance between the center of the bubble and the cell H is also examined in this work. Three selected experiments representative for the observed trends are shown.

Figure 2 shows an example of a cell and an oscillating bubble over a period of 30.6 µs. The camera can record at high framing rates with a reduced resolution. The frame number is indicated at the bottom of each frame. As the full bubble is too large to be captured in one frame, we only show part of it as a slightly curved line in each frame, representing the advancing and receding interface of the oscillating bubble. The images were recorded at 360,000 frames per second with an exposure time of 0.37 µs; thus the time interval between the frames is 2.78 µs. The cell is located at a distance of H = 84 µm from the laser bubble generation point. The bubble reaches its maximum radius of R_m = 100 µm in Frame 4. Initially, the cell moves upwards, possibly exhibiting some deformation. When the bubble collapses (from Frame 5 onwards) a distinct elongation of the cell is observed. Although the shape of the elongated cell is not symmetric, the oscillating bubble clearly has caused strong deformation of the cell. With our current understanding of soft matter, an explanation for this elongation is not immediately clear.

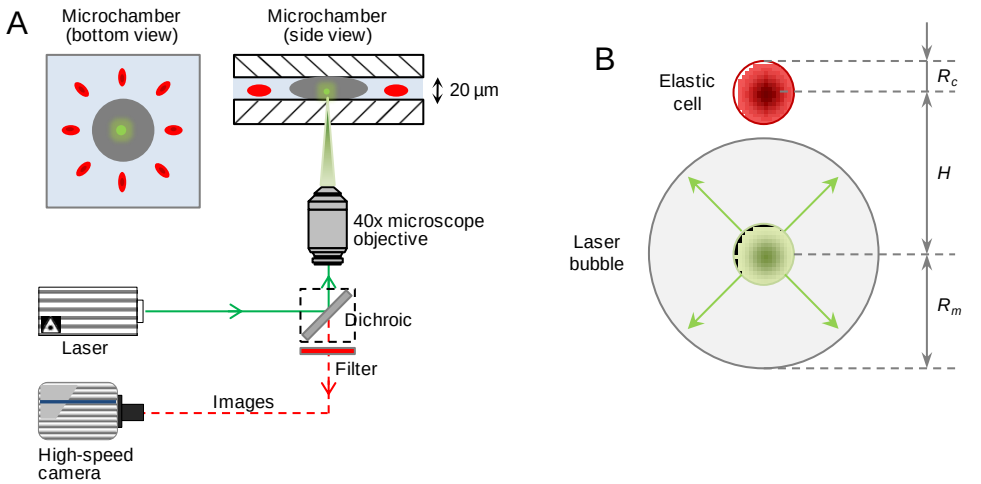

Fig. 1 Schematic of the bubble-cell configuration. (*A*) Schematic of the experimental setup for stretching red blood cells with a laser bubble. The microfluidic chamber has a dimension of 22 × 40 mm^2. The height of the chamber is 20 µm. A pulsed laser is focused at the bottom of the chamber to create a bubble. The bubble dynamics and cell deformation are recorded using a high-speed camera. (*B*) Illustration of an oscillating bubble (bottom) with maximum bubble radius R_m next to an initially spherical vesicle (cell) with radius R_c, located at a centre-to-centre distance of H.

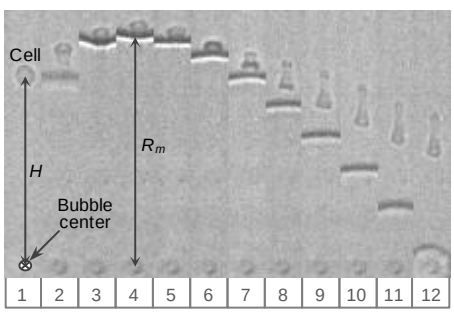

Fig. 2 Relatively large bubble expands near a red blood cell. The image consists of 12 frames taken at an interval of 2.78 µs (360,000 fps) and shutter time of 0.37 µs. The width of each frame is 16 µm. The numbers below the image refer to the frame number. The bubble boundary is visible as a black curved-line. The bubble is generated at the bottom of the frame (indicated as "bubble center" in Frame 1). The cell with a radius of R_c = 4 µm is initially placed at a distance H = 84 µm from the bubble center. The maximum bubble radius R_m = 100 µm is reached at Frame 4 (t = 11.1 µs). The cell is seen to stretch upon bubble collapse (from Frame 7 onwards).

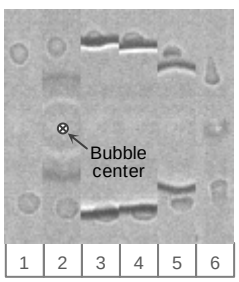

Fig. 3 A small bubble expands near two cells. The maximum bubble radius is R_m = 37 µm. The approximate radius of both cells is R_c = 4 µm. The initial distances of the cell from the bubble center are H = 30 µm (top) and 33 µm (bottom). The frame interval is 2.78 µs (360,000 fps). The width of each frame is 16 µm. The numbers below the image refer to the frame number. Both cells exhibit stretching after the bubble has collapsed (last frame).

Another example is shown in Fig. 3. Here, two cells are present and the laser bubble is generated in between them. Both cells have a radius of about R_c = 4 μm. The first frame is taken immediately before the laser bubble was created. In the second frame the bubble can be seen to expand halfway towards the two cells. Both cells are slightly displaced away from the oscillating bubble but do not seem to exhibit much deformation. In the third frame, the bubble has reached its maximum size of R_m = 37 μm. It is not clear if the cells are deformed, but they probably are squeezed in the vertical direction (thus having a greater horizontal size than vertical size). In Frame 5 this squeezing can clearly be observed. In the last frame, however, the deformation is reversed and the cells are being elongated in the vertical direction. Both cells exhibit more or less the same behaviour. The phenomena observed are qualitatively similar to the ones observed in Fig. 2. Many more experiments were performed and all showed similar behaviour. The cells were always observed to elongate towards the final stage of the bubble collapse, as long as the cells were located relatively close to the oscillating bubble. A cell which is located at a larger distance will be shown in the next example.

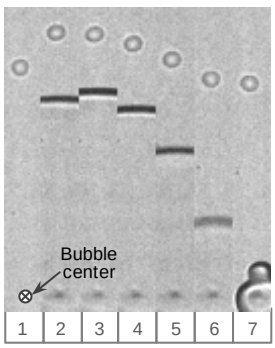

Fig.4 In this particular case the bubble is expanding relatively far away from the cell ($R_m < H$). The maximum bubble radius is R_m = 83 μm and the cell radius is R_c = 3.3 μm. The initial distance is H = 93 μm and the frame interval is 4 μs (250,000 fps). The width of each frame is 16 μm. The numbers below the image refer to the frame number. The cell is displaced by the oscillating bubble, but returns to its original position without any apparent stretching.

In Fig. 4, a cell is placed at a larger distance of H = 93 μm (the maximum bubble radius is R_m = 83 μm). The cell has a radius of R_c = 3.3 μm. The first frame is taken again right before the laser bubble is generated. As in the previous figures, the black line shows the advancing front of the bubble. In the second frame, the bubble is pushing the cell upwards. In the third frame, the bubble has reached its maximum size. When the bubble collapses, the cell remains spherical and no obvious deformation is observed. This example seems to indicate that the distance H (or rather the dimensionless distance H/R_m), plays a crucial role in the occurrence of cell stretching.

In the previous examples, we have observed cell stretching and only a few typical examples from numerous experiments performed are shown. The physical mechanism behind this stretching of the cell is still unclear at this point. In the next section, the underlying mechanism will be investigated through numerical simulations.

2.2 Numerical results using the boundary element method

In order to get a better understanding of the physics involved, numerical simulations based on a boundary element code[16,17] were performed. The oscillating bubble is modelled as a vapour bubble (no gas contents). The shape of the bubble wall is determined by the surrounding fluid. This fluid contains a liquid vesicle which represents the cell. Its contents are a second fluid and its boundary has elastic properties. Due to the oscillation of the bubble, the surrounding fluid is set in motion. This in turn will set the cell contents in motion and during this motion the cell will deform. Since the phenomena observed are mainly of inertial origin, the fluids are being modelled as a potential flows. A boundary element method is used such that only a mesh on the bubble surface and the cell surface are needed. Both fluids (the main fluid and the fluid inside the cell) are modelled separately. They are coupled to each other through the boundary conditions on the cell surface,[18,19] which are continuity of the normal velocity and normal stress. In our case, a simple membrane tension model is used. For more details the reader is referred to Appendix B. The numerical model is modified from Klaseboer and Khoo;[18,19] but the implementation is given here in a more concise and straightforward form.

Important parameters considered in this model are the maximum bubble radius R_m, the cell radius R_c, the initial distance between the centers of the bubble and the cell H, and the membrane tension σ. The following four dimensionless parameters are then obtained: the ratio of cell size and maximum bubble size R_c/R_m, the (initial) distance of the centres of the cell and the bubble $H' = H/R_m$, and finally an elasticity parameter $K = \sigma/(R_c p_\infty)$, with p_∞ the reference pressure far away from the bubble (atmospheric pressure). The density ratio of the two fluids involved (ρ_1 for water and ρ_2 for the cell contents) is very close to unity: $\alpha = \rho_1/\rho_2 = 1.0$. See Appendix B for more details.

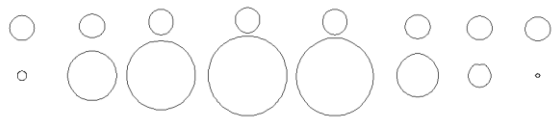

Fig. 5 Numerical simulation of a bubble near a 'rigid' cell. The cell is shown on top and the oscillating bubble at the bottom. Eight frames of the simulation results are shown here (with increasing time from left to right). The parameters are H'=1.15, R_c/R_m=0.3, K=1.33, α=1.0. The cell exhibits slight oscillations (barely visible in the plot), but does not deform much. The bubble almost collapses spherically. The oscillation time (time from inception of the bubble to collapse) is given by twice the Rayleigh collapse time[22,23] and is related to the maximum bubble radius R_m as: $t_{osc} = 2 \times 0.915 R_m \sqrt{\rho_1/p_\infty}$ (see also Eq. 6).

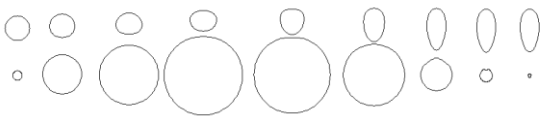

Fig. 6 Numerical simulation of a bubble near a 'floppy' cell. H'=1.15, R_c/R_m=0.3, K=0.067, α=1.0. The bubble (bottom) expands, deforms the cell (top) and pushes it upwards slightly. Around the maximum size of the bubble, the cell tries to restore its spherical shape, helped to do so by the low pressure around the bubble (the pressure inside the bubble is zero). It overcorrects itself and gets sucked into the collapsing bubble flow resulting in a stretched cell. Depending on the elastic properties of the cell, it will regain its spherical shape or stay deformed permanently.

In order to investigate the physics of the problem, three simulation cases will be shown first. These three cases are representative for the phenomena observed and will reveal the physics involved. For all three cases, the cell is relatively large, i.e. $R_c/R_m = 0.3$; thus the maximum bubble size is about three times the cell size. The first case, shown in Fig. 5, shows an oscillating bubble near a cell with a rather rigid membrane K=1.33. Due to its high membrane tension, the cell does not deform very much during the bubble oscillation. The cell is pushed slightly upwards during the expansion of the bubble and moves downwards again during the bubble collapse. It is thus as if the cell is acting as an almost rigid particle. This is entirely due to the membrane tension that tends to keep the shape of the cell unchanged. The bubble remains almost spherical during the whole oscillation cycle, but some slight deviations from sphericity can be observed during the later stages of the oscillation. The cell retains its original volume throughout the simulation, since the liquids are incompressible due to the assumption of potential flow.

The next case, shown in Fig. 6, exhibits a totally different behaviour. All the parameters are similar to the case of Fig. 5, but K=0.067 instead of K=1.33. Thus the elasticity is 20 times smaller than in the previous case. As a result, cell deformation during the expansion phase of the bubble is observed. When compared to Fig. 5, the cell is flatter when the bubble approaches its maximum volume (see Frame 3). The cell, which is now much more 'floppy' tries to regain its original spherical shape and the bottom of the cell is approaching the bubble at a much closer distance during this process. It overcorrects itself helped by the zero pressure inside the bubble. When the bubble collapses, the bottom part of the cell is drawn downwards towards the collapsing cell (last 5 frames). The final result is a very elongated cell, as opposed to the spherical cell of Fig. 5 (last frame).

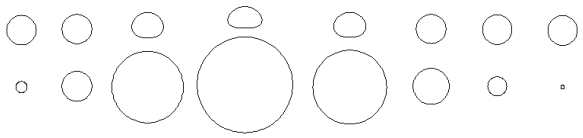

Fig. 7 Numerical simulation of a bubble (bottom) near a 'neutral cell' (top) with no interfacial tension (K=0), H'=1.15, R_c/R_m=0.3, α=1.0. The cell deforms, but regains exactly its initial position and shape upon bubble collapse.

From the previous simulation, it might be concluded that a lower membrane tension would always result in an elongated cell towards the end of the bubble collapse. This, however, is not the case. In another typical case, the membrane tension has been set to zero and thus K=0.0 (Fig. 7). During the expansion of the bubble, the cell deforms much more than in Fig. 6 (see for example Frame 4). However, due to the lack of membrane tension, the cell does not 'relax' during this stage and merely follows the flow generated by the bubble. During the collapse phase of the bubble, it reverts back to its original spherical shape. From this last example, it can thus be concluded that a certain amount of membrane tension is required to observe phenomena as shown in Figs. 3 and 4. Excessive or too little tension will not produce the typical 'stretching' of the cell as observed in the experiments. The observed deformation seems to be around its maximum value for K~0.07, but significant stretching occurs for K=0.01 to 0.25 (while keeping the other parameters constant, i.e. H'=1.15, R_c/R_m=0.3 and α=1.0).

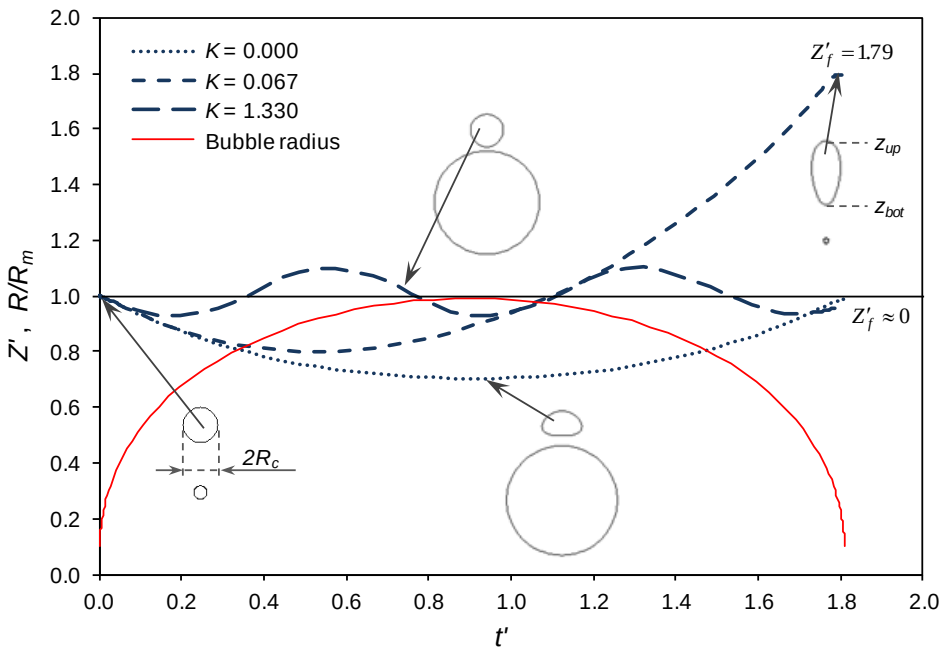

Fig 8. The relative vertical deformation of the cell, Z', for the three cases shown in Figs. 5, 6 and 7, defined as $Z' = (z_{up} - z_{bot})/2R_c$ as a function of dimensionless time $t' = t/(R_m\sqrt{\rho_1/p_\infty})$. The parameters are H'=1.15, R_c/R_m=0.3 and α=1.0. A value of Z'>1 indicates elongation in the vertical direction, a value Z'<1 indicates contraction in the vertical direction. The cell with K=0.00 deforms, but finally ends up at Z'=1.0. The cell with K=0.067 ends up with the largest deformation. The cell with K=1.33 oscillates several times, but with a much lower amplitude than the other two cases. Some snapshots of bubble and cell shapes are given as well (the lines indicate the time where the image was taken). The bubble radius-time plot is also given (numerical results).

In order to investigate in more detail the physics involved, in Figure 8 we have plotted the nondimensional stretching (vertical deformation) of the cell defined as:

$$Z' = \left(z_{up} - z_{bot}\right)/2R_c \qquad (1)$$

z_{up} indicates the top vertical position of the cell (see upper right part of Fig.8), while z_{bot} indicates the bottom position. The difference between these two quantities has been made dimensionless with twice the cell radius and is called Z'. A value of Z' larger than one indicates elongation, while a value lower than one indicates contraction. As can be observed in Fig. 8, the cell with K=0.00 shows contraction during the whole bubble oscillation period and never reaches Z'>1. The cell with K=0.067 contracts during the expansion part of the bubble, but then quickly reaches values of Z' larger than one. The cell with K=1.33 shows another interesting behaviour, it oscillates several times during the bubble lifetime. The higher the value of K, the more oscillations can be observed (not shown).

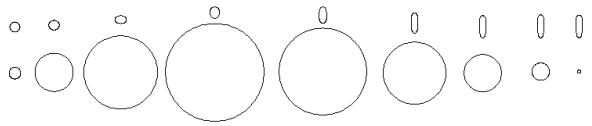

Fig. 9 Numerical simulation of an oscillating bubble near a cell with a size of 1/10th the maximum bubble size (R_c/R_m=0.1); the other parameters are K=0.015, H'=0.91 and α=1.0. The cell exhibits severe stretching during bubble collapse. The bubble oscillates almost spherically. This severe cell stretching does not always appear, but only for specific ranges of H' and K.

After presenting results for the relatively large vesicle size in Figs. 5-8, we will now investigate a vesicle which has 1/10 the size of the maximum bubble radius (R_c/R_m=0.1). This value corresponds more with the experiments (Figs. 2-4). Figure 9 shows a typical example of the simulation results. In the first frame, the bubble is still very small. While the bubble grows to its maximum size in Frame 4, the cell first flattens slightly (Frame 3), before elongating towards the bubble in Frame 4. While the bubble collapses (Frames 5 to 9), the cell stretches. The cell retains its original volume (as in all the simulations shown here). When the other parameters are kept constant: R_c/R_m=0.1, H'=0.91 and α=1.0, while K is changed, it is observed that stretching occurs roughly from K=0.002 to 0.03. For values of K<0.002, the cell just follows the flow (very similar to Fig. 7) and for values K>0.03 the cell becomes too rigid to exhibit much deformation (very similar to Fig. 5). A more detailed systematic study of the final deformation as a function of the parameters involved will be given in Section 3.

3. Discussion

From the experimental observations and the numerical simulations of Section 2, it becomes clear that the elasticity of an object plays a crucial role in determining whether it stretches. The experiments of Quinto-Su *et al.*[20] used a single laser-induced cavitation bubble to quantify the deformability of red blood cells with different elasticity properties. The cells with higher elasticity (for example: the neuraminidase treated cells) took longer to recover their shape from their maximum deformation compared to normal or more rigid cells (for example: the wheat-germ-agglutinin treated cells). The initial elongation of the cells, which is due to the fast oscillating bubble, depends on the initial distance between the cell and the bubble. Our numerical models and experimental evidences also reveal that the bubble dynamics significantly affects the deformation of the cells or other elastic objects.

From a fluid dynamics point of view, the oscillating bubble is essentially a source/sink depending on whether it is expanding or contracting respectively. This explains why the cell in Fig. 7 will revert back to its original spherical shape. Within the present computational model, stretching occurs after surface tension causes the cell to relax and overshoot its equilibrium shape, during the time when the bubble edge is both near its maximum size and in close proximity to the cell. The side facing the bubble thereby moves closer to the bubble and gets dragged with the flow during the collapse of the bubble.

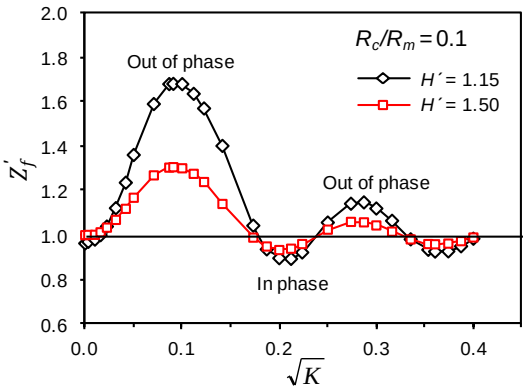

Fig. 10. Numerical predictions of the final deformation (at the moment of bubble collapse) Z_f' as defined in Eq.2 as a function of $\sqrt{K}$ for R_c/R_m=0.1 and for two values of H' (H'=1.15 and H'=1.5). Z_f' shows a maximum elongation at $\sqrt{K} \approx 0.1$, then a negative minimum (contraction) around $\sqrt{K} \approx 0.2$ and another maximum around 0.3. The maxima and minima roughly correspond to the bubble and cell being out or in phase with each other.

We will now study the stretching of the cell in a more systematic manner in Figs. 10 and 11. The final deformation Z_f' is defined as:

$$Z_f' = Z'(t = t_{osc}) \qquad (2)$$

as indicated in Fig. 8 (e.g. Z_f'=1.79 for K=0.067, $Z_f'\approx$0 for K=1.33 and K=0.0). In Fig. 10, the value R_c/R_m=0.1 is fixed and K is changed. Two values of H' are plotted (1.15 and 1.5, i.e. the cell is located very near and at some distance from the bubble). The results show that for very low values of K, the cell just follows the flow. There is a value of K for which a maximum Z_f' is observed, i.e. $\sqrt{K} \approx 0.1$, followed by a negative minimum (the cell is then not stretched but squeezed) and more maxima and minima. The subsequent maxima and minima are getting lower and lower. As could be expected the effect is more pronounced for H'=1.15 than for H'=1.5, since the cell is much nearer to the bubble for H'=1.15. Except for the amplitude, the nature of the two curves for H'=1.15 and H'=1.5 is very similar. Fig. 11 shows the analogous relationship between final deformation Z_f' and $\sqrt{K}$, but now for R_c/R_m=0.3. The results are very similar to those of Fig. 10, except for a rescaling of the horizontal axis by a

factor close to 3. The final graph of this parametric study is shown in Fig. 12 and shows the value of Z_f' as a function of H' for two different values of K. The final deformation very rapidly increases when H' decreases towards 1.0. When H' becomes larger than 3, the final deformation is very small ($Z'\approx 1.0$).

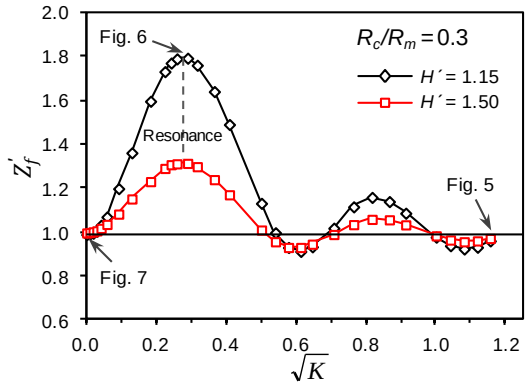

Fig. 11 Numerical predictions of the final deformation (at the moment of bubble collapse) Z_f' as defined in Eq.2 as a function of $\sqrt{K}$ for R_c/R_m=0.3 and for two values of H' (H'=1.15 and H'=1.5). The datapoints corresponding to Figs.5-7 are indicated with arrows. The blue vertical line indicates the value $\sqrt{K_{res}}$, the square root of the 'resonance' value of K, which coincides for both H'=1.15 and H'=1.5. The subsequent minima and maxima are not exactly aligned. The gross features resemble very much those of Fig. 10, with a scaling factor of about 3 difference in the horizontal axis as predicted by Eq. 7.

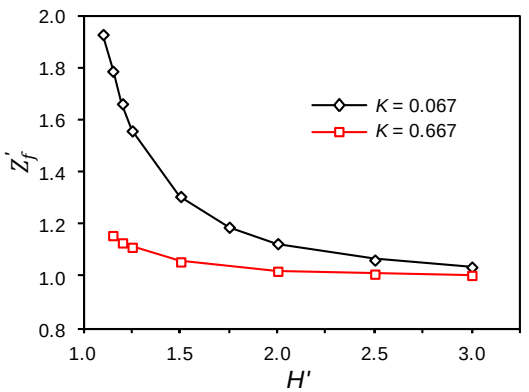

Fig. 12 Final deformation Z_f' as a function of H' (with K kept constant at K=0.067 and K=0.667). Z_f' sharply increases when H' approaches 1.0 (numerical results).

We will now try to explain the observed behaviour of Figs. 10-12 in a more quantitative manner. Lamb[21] described small oscillations of a drop of liquid about a spherical form (initial radius R_c) and density ρ_2 surrounded by another liquid with density ρ_1 and interfacial tension σ. This theory turns out to be helpful to understand the physics involved in the current cell elongation phenomenon. He then finds (here expressed in the oscillation time, t_c of such a drop instead of his angular frequency):

$$t_c = 2\pi\sqrt{\frac{R_c^3\left[(n+1)\rho_2 + n\rho_1\right]}{\sigma n(n+1)(n-1)(n+2)}} \qquad (3)$$

Lamb further states that the most important mode of vibration is that for which $n = 2$, which gives $t_c = \pi\sqrt{(R_c^3[3\rho_2 + 2\rho_1])/(6\sigma)}$, which in the current framework with $\rho_2 = \rho_1$ can be further simplified to

$$t_c = R_c\pi\sqrt{\frac{5R_c\rho_1}{6\sigma}} \qquad (4)$$

This can be expressed with the help of the elasticity parameter $K = \sigma/(R_c p_\infty)$ introduced earlier as:

$$t_c = R_c\pi\sqrt{\frac{5\rho_1}{6Kp_\infty}} \qquad (5)$$

On the other hand, the oscillation time of the bubble is given by[22,23]

$$t_{osc} = 2\times 0.915 R_m\sqrt{\rho_1/p_\infty} \qquad (6)$$

The balance between Eqs. 5 and 6 now plays a crucial role in determining the stretching of the cell. As we have seen in Fig. 8, the cell can oscillate several times during the bubble lifetime. It looks like the maximum deformation of the cell occurs when the oscillation time of the bubble is about half the oscillation time of the drop, i.e, $t_{osc}\approx t_c/2$. That is, when the bubble and cell are out of phase (see Fig.10). Using this information in Eqs.4 and 5 will give rise to the following relationship between R_c/R_m and the value of K where resonance will occur, termed here as K_{res}:

$$\frac{R_c}{R_m} = \frac{4\times 0.915}{\pi}\sqrt{\frac{6}{5}K_{res}} = 1.28\sqrt{K_{res}} \qquad (7)$$

The observed difference of a factor of 3 in Figs.10 and 11 now becomes apparent, since R_c/R_m was 0.1 in Fig. 10 and 0.3 in Fig. 11. Thus according to Eq. 7, $\sqrt{K_{res}}$ should also exhibit a factor of 3 between these two figures. Through a similar procedure as the one shown above to derive Eq.7, we can get the subsequent minima and maxima shown in Figs.10 and 11, with $t_{osc}\approx t_c$ (i.e. in phase; corresponding to the minimum in Figs. 10 and 11) and $t_{osc}\approx 3t_c/2$ (out of phase once more). It should be mentioned that the calculated values do not exactly correspond to the values from the theory as could hardly be expected from this simple theory for the higher order in and out of phase cases. Nevertheless, the value of K_{res} of Eq. 7 seems to be given rather accurately (at least for the values tested here).

The confined geometry of the microchamber allows the cells to be kept in the depth of field of the camera during the rapid flow events. Therefore, it is possible to study the mechanism behind the stretching of the cell near the oscillating bubble. In the experiments, due to the height constraints of the microchannel (20 µm), there will most likely be some 2D effects. Nevertheless, the authors believe that the essential physics are the same for the experiments and the numerical simulations (which are in 3D). In biological or medical applications utilizing cells, the cell will also most likely be in 3D-environments.

Considering the cell as an object with a membrane tension alone, is of course an approximation. Nevertheless, an indication of the value of this tension can be obtained from an article by Colbert *et al.*[24]; in which they measure membrane tensions of about 3.5 nN/µm, which is about twenty times smaller than the surface tension of water (~73 mN/m). The dimensionless value of

the elasticity parameter would be $K = \sigma/(R_c p_\infty) \approx 0.01$. This value lies in the range of K=0.002 to 0.025, for which significant stretching was observed in the example of R_c/R_m=0.1 and H'=0.91 (Fig. 8). Finally, stretching only occurs for a range of K values; K should not be too large or too small for stretching to occur.

The current theory might also explain why in the experiments of Chen *et al.*[25], in experiments of blood vessels with ultrasonic cavitation, vessel invagination towards oscillating bubbles occurred (i.e. the vessel walls were attracted towards the oscillating bubble). A similar mechanism as the one shown here could very well be the explanation for this phenomenon, since the blood vessels also exhibit some elastic properties, very similar to the cells that are studied in the current article. The vessel will bulge outwards during bubble expansion, relax towards the bubble due to its elasticity around the maximum bubble size and finally get sucked towards the bubble during the collapsing phase of the bubble.

4. Conclusions

It has been shown, both through experiments and numerical simulations, that the elasticity of an object (a cell in this case) plays a crucial role for the stretching of such an object when it interacts with an oscillating bubble. A typical example with red blood cells clearly illustrated the physics involved. During the expansion phase of the bubble, a nearby cell will be deformed. When the bubble has reached its maximum volume, the cell tries to recover its original shape due to the elasticity that it possesses. The part of the cell exposed to the bubble will move slightly towards the bubble during this process. When the bubble subsequently collapses, this part will be sucked in the flow generated around the bubble. This explains the elongation observed in the cell.

It has also been shown that extremely floppy objects (with very low elastic properties) will just follow the flow and end up in exactly the same state after the bubble has disappeared as where they were before the oscillating bubble appeared. Extremely elastic objects (i.e. almost rigid objects) will also not exhibit any stretching behaviour. A realistic criterion to calculate the value for which maximum stretching occurs (Eq. 7) is proposed in this work. The optimal 'resonance' occurs when the oscillation period of the object is twice the bubble lifetime. Cell stretching (and likely other related phenomena such as emulsification with ultrasound) is most effective for resonant oscillations.

Acknowledgements

This work is supported by the Agency for Science, Technology and Research (A*STAR) through the JCO Grant no. 10/03/FG/05/02.

Appendix A: Experimental setup

The experiments were conducted in a microfluidic system consisting of a microchamber and a frequency doubled Nd:YAG laser (Orion, New Wave Research, USA), shown in Fig. 1*A*. The microchamber is made of two #1 microscope cover slips (22 mm × 40 mm) separated by aluminium spacers with a thickness of 20 μm. The cover slips and spacers are clamped by a homemade precision holder with rubber fitted fastener on their edges, creating a microfluidic chamber with a height of the spacers' thickness. A high-speed camera (Fastcam SA1.1, Photron, Japan) connected to an inverted microscope (IX71, Olympus, Japan) with a 40× water immersion objective lens (Olympus, Japan) was used to record the rapid flow events and stretching of the cells in the microchamber.

Human erythrocytes or red blood cells (RBCs) were drawn into an Eppendorf microcentrifuge tube and suspended in PBS (phosphate buffered saline) buffer with 0.1% BSA (bovine serum albumin). The suspension was centrifuged and the pellets were washed with the buffer three times. The cells were then diluted with the buffer before depositing them into the microchamber for the experiments.

A laser pulse at 532 nm with duration of 6 ns was focused at the liquid gap in the microchamber at a certain distance from a single cell. The high intensity of the laser pulse at the focal volume causes an optical breakdown, which leads to the formation of the cavitation bubble. The bubble expands rapidly, reaches its maximum radius of 30-100 μm and subsequently collapses. The maximum size of the bubble is controlled by varying the laser energy. The bubble dynamics and the stretching of the cell were recorded by a high-speed camera at a speed up to 360,000 frames per second and an exposure time of 0.37 μs.

Appendix B: Numerical model

An incompressible and inviscidflow (the Reynolds number for the oscillating bubble system is much larger than one) can be shown to obey the Laplace equation (potential flow). Numerically, instead of meshing the whole fluid domain, it is advantageous to use the analogous approach with a direct boundary integral equation over the whole boundary of the problem, S, as:[26]

$$\Omega(\underline{x}_0)\phi(\underline{x}_0) + \int_S \phi(\underline{x}) \frac{\partial G(\underline{x}, \underline{x}_0)}{\partial n} dS = \int_S G(\underline{x}, \underline{x}_0) \frac{\partial \phi(\underline{x})}{\partial n} dS \qquad \text{(B1)}$$

Here, ϕ is the potential and $\partial\phi/\partial n$ the normal velocity at the surface S (with $\partial/\partial n = \underline{n}\cdot\nabla$ and $\underline{n}$ the normal vector at the surface). G is the so-called Green's function, which is $G = 1/|\underline{x} - \underline{x}_0|$ in this case, and $\partial G/\partial n$ is its normal derivative. $\underline{x}_0$ is the point under consideration and $\underline{x}$ is the vector pointing to a location on S over which the integration is done. $\Omega(\underline{x}_0)$ takes on different values if $\underline{x}_0$ is situated in the fluid domain, on the surface of the fluid domain, S, or outside the fluid domain:

$$\Omega(\underline{x}_0) = \begin{cases} 4\pi, \text{if } \underline{x}_0 \text{ inside the fluid} \\ \text{solid angle, if } \underline{x}_0 \text{ on S} \\ 0, \text{if } \underline{x}_0 \text{ outside the fluid} \end{cases} \qquad \text{B2)}$$

In what follows we will simplify the notation by omitting $\underline{x}_0$ and $\underline{x}$ and write $H = \partial G/\partial n$ and $v = \partial\phi/\partial n$. In order to correctly describe the physics, we must assume two fluids, 1 and 2. In fluid 1 the bubble and the cell reside (here water) and it assumed to extend to infinity. Fluid domain 2 consists of the internal fluid of the cell, which is separated from fluid 1 by a membrane. We assume further that potential flow holds in both fluids, thus:

$\nabla^2\phi_1 = 0$ in Fluid 1 and $\nabla^2\phi_2 = 0$ in Fluid 2. For any point on the bubble surface (the subscript 'b' indicates the bubble and 'c' the cell, subscript '1' refers to Fluid 1 and '2' to Fluid 2):

$$\Omega_b \phi_{1b} + \int_b H_{bb}\phi_{1b}\,dS + \int_c H_{bc}\phi_{1c}\,dS = \int_b G_{bb}v_{1b}dS + \int_c G_{bc}v_{1c}dS \tag{B3}$$

Note that the surface over which is integrated consists of two separate surfaces: the bubble surface and the cell surface. The first integrals indicate the influence of the bubble on itself and the second integrals the influence of the cell on the bubble. For any point on the cell surface at the Fluid 1 side, we similarly can write:

$$\Omega_c \phi_{1c} + \int_b H_{cb}\phi_{1b}\,dS + \int_c H_{cc}\phi_{1c}\,dS = \int_b G_{cb}v_{1b}dS + \int_c G_{cc}v_{1c}dS \tag{B4}$$

and on the Fluid 2 side of the cell (since the bubble is not part of Fluid 2 it does not appear in the integrals):

$$(4\pi - \Omega_c)\phi_{2c} - \int_c H_{cc}\phi_{2c}dS = \int_c G_{cc}v_{2c}dS \tag{B5}$$

The factor $4\pi - \Omega_c$ appears since the combined angle viewed from both fluids must be 4π. The normal velocity must be continuous across the cell, otherwise gaps or overlapping areas will appear after a while, thus $v_{1c} = -v_{2c}$. A minus sign appears here since the normal vectors in Fluids 1 and 2 are pointing in the opposite direction with respect to each other; this is also the reason why a minus sign appears in the first integral of Eq. B5. When Eqs. B4+B5 are added we get:

$$\begin{aligned} &4\pi\phi_{2c} + \Omega_c(\phi_{1c} - \phi_{2c}) + \int_b H_{cb}\phi_{1b}\,dS \\ &+ \int_c H_{cc}(\phi_{1c} - \phi_{2c})dS = \int_b G_{cb}v_{1b}dS \end{aligned} \tag{B6}$$

The potentials at both sides of the cell show jumps in general. For any point outside Fluid 2, Ω=0 (Eq.B2). If this point is taken to coincide with a location on the bubble surface, then the same terms H_{bc} and G_{bc} appear as in Eq. B3 and we can easily find the following relationship:

$$-\int_c H_{bc}\phi_{2c}\,dS = \int_c G_{bc}v_{2c}dS \tag{B7}$$

The normal vector in Fluid 2 is in the opposite direction, thus a minus sign appears. Using again $v_{1c} = -v_{2c}$, we get: $\int_c G_{bc}v_{1c}\,dS = \int_c H_{bc}\phi_{2c}\,dS$, which can be used to replace the last integral of Eq.B3 and will result in:

$$\Omega_b \phi_{1b} + \int_b H_{bb}\phi_{1b}\,dS + \int_c H_{bc}(\phi_{1c} - \phi_{2c})dS = \int_b G_{bb}v_{1b}dS \tag{B8}$$

The velocity vectors in both Fluids are indicated as: $\underline{u}_1 = \nabla\phi_1$ and $\underline{u}_2 = \nabla\phi_2$. On the cell surface, we can apply the Bernoulli equation at each side of the cell boundary to get for Fluid 1 and Fluid 2 respectively:

$$\rho_1 \frac{D\phi_{1c}}{Dt} = p_\infty - p_{1c} + \frac{1}{2}\rho_1\left|\underline{u}_{1c}\right|^2 \tag{B9}$$

$$\rho_2 \frac{D\phi_{2c}}{Dt} = p_\infty - p_{2c} - \frac{1}{2}\rho_2\left|\underline{u}_{2c}\right|^2 + \rho_2\underline{u}_{1c}\cdot\underline{u}_{2c} \tag{B10}$$

In order to be consistent, the material derivative D/Dt must be defined identically in both fluids; later, the nodes of the mesh will be chosen to follow Fluid 1; thus $D/Dt = \partial/\partial t + \underline{u}_1\cdot\nabla$. This leads to different terms in Eq. (B10). The densities are ρ_1 for the surrounding fluid (water) and ρ_2 for the cell contents. Furthermore we assume that a membrane tension exists across the surface due to the elasticity of the cell[24] as

$$p_{2c} - p_{1c} = \sigma\kappa \tag{B11}$$

with σ the membrane tension and κ the local curvature of the cell. This formulation is very similar to the formulation of interfacial tension in drops and bubbles. Although much more complicated models could be used,[27] we prefer to keep the model as simple as possible, yet retaining the main physics involved. A relationship can now be obtained between the potentials at both sides of the cell by using Eqs. B9-B11.

$$\frac{D(\rho_2\phi_{2c} - \rho_1\phi_{1c})}{Dt} = -\frac{1}{2}\rho_2\left|\underline{u}_{2c}\right|^2 + \rho_2\underline{u}_{1c}\cdot\underline{u}_{2c} - \frac{1}{2}\rho_1\left|\underline{u}_{1c}\right|^2 - \sigma\kappa \tag{B12}$$

This equation will provide us the necessary relationship between the potentials at both sides of the cell. A simple time discretisation (assuming that all terms on the right hand side of Eq. B12 are known from the previous time step t-Δt) and introducing the density ratio $\alpha = \rho_1/\rho_2$ and a function F will lead to:

$$\begin{aligned} F &= \phi_{2c} - \alpha\phi_{1c} = (\phi_{2c} - \alpha\phi_{1c})_{t-\Delta t} \\ &+ \Delta t\left[-\frac{1}{2}\left|\underline{u}_{2c}\right|^2 + \underline{u}_{1c}\cdot\underline{u}_{2c} - \frac{1}{2}\alpha\left|\underline{u}_{1c}\right|^2 - \frac{\sigma\kappa}{\rho_2}\right]_{t-\Delta t} \end{aligned} \tag{B13}$$

Here, the subscript t-Δt indicates quantities taken at the previous time step. Using the definition of F, we can now replace ϕ_{2c} in Eq.B8 and Eq.B6 and obtain:

$$\begin{aligned} &\Omega_b \phi_{1b} + \int_b H_{bb}\phi_{1b}\,dS + (1-\alpha)\int_c H_{bc}\phi_{1c}dS \\ &- \int_c H_{bc}F dS = \int_b G_{bb}v_{1b}dS \end{aligned} \tag{B14}$$

$$\begin{aligned} &4\pi\alpha\phi_{1c} + (4\pi - \Omega_c)F + \Omega_c(1-\alpha)\phi_{1c} + \int_b H_{cb}\phi_{1b}\,dS \\ &+ (1-\alpha)\int_c H_{cc}\,\phi_{1c}dS - \int_c H_{cc}\,F dS = \int_b G_{cb}v_{1b}dS \end{aligned} \tag{B15}$$

The Bernoulli equation can also be applied at the bubble-fluid surface, thus (with p_b the pressure inside the bubble):

$$\rho_1 \frac{D\phi_{1b}}{Dt} = p_\infty - p_b + \frac{1}{2}\rho_1\left|\underline{u}_{1b}\right|^2 \tag{B16}$$

On the bubble surface, after a discretisation with time similar to Eq.B13, Eq.B16 will provide us with the potential ϕ_{1b}, and the normal velocity v_{1b} is the unknown quantity to be calculated. We will assume here that the pressure inside the bubble is zero (p_b=0) (it thus behaves as a vapour bubble which seems to be consistent with the experimental observations as no rebound is observed). As initial condition we give $\phi_{1b}(t=0) = -2.580697$, while the radius of the bubble is R_0=0.1R_m, with R_m the maximum bubble radius.

The numerical implementation is identical to the ones used in Klaseboer and Khoo.[18,19] An axial symmetric formulation has been used similar to those of Wang *et al.*,[16,17] since the effects of gravity can be ignored. After discretizing the bubble and cell surface with nodes and linear elements, initially a system of linear equations appears as:

$$\begin{bmatrix} \underline{\underline{\Omega}}_b + \underline{\underline{H}}_{bb} & \underline{\underline{H}}_{bc} \\ \underline{\underline{H}}_{cb} & \underline{\underline{\Omega}}_c + \underline{\underline{H}}_{cc} \end{bmatrix} \cdot \begin{bmatrix} \underline{\phi}_{1b} \\ \underline{\phi}_{1c} \end{bmatrix} = \begin{bmatrix} \underline{\underline{G}}_{bb} & \underline{\underline{G}}_{bc} \\ \underline{\underline{G}}_{cb} & \underline{\underline{G}}_{cc} \end{bmatrix} \cdot \begin{bmatrix} \underline{v}_{1b} \\ \underline{v}_{1c} \end{bmatrix} \qquad \text{(B17)}$$

The upper part of Eq.B17 corresponds to the matrix equivalent of Eq.B3 and the lower part corresponds to Eq.B4. It relates the potentials and the normal velocities of every node to all the other nodes. The matrices $\underline{\underline{H}}$ and $\underline{\underline{G}}$ are called influence matrices. For example $\underline{\underline{H}}_{bb}$ represents the influence of the bubble on itself, while $\underline{\underline{H}}_{bc}$ represents the bubble's influence on the cell, etc. (see for example Becker[26]). $\underline{\underline{\Omega}}_b$ and $\underline{\underline{\Omega}}_c$ are diagonal matrices containing the solid angles of each node for the bubble and cell respectively.

In the current framework, Eq.B17 has been replaced by the matrix equivalent of Eqs.14 and 15:

$$\begin{bmatrix} -\underline{\underline{G}}_{bb} & \underline{\underline{H}}_{bc}(1-\alpha) \\ -\underline{\underline{G}}_{cb} & 4\pi\alpha\underline{\underline{I}} + (1-\alpha)\left(\underline{\underline{\Omega}}_c + \underline{\underline{H}}_{cc}\right) \end{bmatrix} \cdot \begin{bmatrix} \underline{v}_{1b} \\ \underline{\phi}_{1c} \end{bmatrix} = \begin{bmatrix} -\left(\underline{\underline{\Omega}}_b + \underline{\underline{H}}_{bb}\right) \cdot \underline{\phi}_{1b} + \underline{\underline{H}}_{bc} \cdot \underline{F} \\ -\underline{\underline{H}}_{cb} \cdot \underline{\phi}_{1b} + \left(-4\pi\underline{\underline{I}} + \underline{\underline{\Omega}}_c + \underline{\underline{H}}_{cc}\right) \cdot \underline{F} \end{bmatrix} \qquad \text{(B18)}$$

With $\underline{\underline{I}}$ the identity matrix. In Eq. B18, the known quantities, $\underline{\phi}_{1b}$ and $\underline{F}$ have been put on the right hand side. The unknowns, $\underline{v}_{1b}$ and $\underline{\phi}_{1c}$ appear on the left. Note that Eq.B18 will revert to the simulation of a 'normal' oscillating bubble if the cell would not have any elasticity ($\underline{F}$=0) and density equal to water (α=1). The upper part of Eq.B18 would give a relationship between the potential, $\underline{\phi}_{1b}$, and normal velocity, $\underline{v}_{1b}$, on the bubble surface, while the lower part would give the potential at the cell location, $\underline{\phi}_{1c}$, with a solid angle 4π according to Eqs.B1-B2. Finally, Eq.B5 can be rewritten in matrix notation as (in the last equality once more $v_{1c} = -v_{2c}$ has been used)

$$\left(4\pi\underline{\underline{I}} - \underline{\underline{\Omega}}_c - \underline{\underline{H}}_{cc}\right) \cdot \underline{\phi}_{1c} = \underline{\underline{G}}_{cc} \cdot \underline{v}_{2c} = -\underline{\underline{G}}_{cc} \cdot \underline{v}_{1c} \qquad \text{(B19)}$$

In order to make Eq.B9) totally parameter free, the following nondimensionalization was applied;[19] for time $t_0 = R_m\sqrt{\rho_1 / p_\infty}$, for potentials (and F) $\phi_0 = R_m\sqrt{p_\infty / \rho_1}$, for velocities $u_0 = \sqrt{p_\infty / \rho_1}$. The problem then reveals the following four dimensionless parameters, the density ratio $\alpha = \rho_1 / \rho_2$, the ratio of cell size vs. maximum bubble size R_c / R_m, the (initial) distance of the centres of the cell and the bubble $H'=H/R_m$, and finally an elasticity parameter $K = \sigma/(R_c p_\infty)$. The influence of the elasticity will appear as $K\alpha(R_c / R_m)$ in the nondimensional form of Eqs. B13-B15. The density ratio of the two fluids involved (water and the cell contents) is very close to unity and thus throughout the simulations shown here a value of $\alpha = 1.0$ has been used. A value slightly different from 1.0 (1.1 and 0.9) did not give any significantly different results. It is therefore assumed that the density ratio is not a parameter for this particular problem.

The numerical procedure consists of the following steps:

1) Calculate the velocity vectors occurring in Eqs. B13 and B16. For example $\underline{u}_{1b}$ can be obtained from the normal velocity at a node v_{1b} and from the distribution of the potential on the surface, ϕ_{1b}, the tangential velocity can be obtained. From the normal and tangential components of the velocity, the velocity vector can be calculated. The curvature has been calculated with the help of a tangent angle $\tan\theta = dz/dr$ (with z the vertical coordinate and r the radial coordinate of the axial symmetric system), such that the curvature can be written as $\kappa = \sin\theta/r + d\theta/ds$ (with s the arc length across the cell boundary, Chesters[28])
2) The vectors $\underline{\phi}_{1b}$ and $\underline{F}$ in Eq.B18 are now known and the right hand side of the equation can be obtained.
3) Eq.B18 can be solved for the unknown normal velocities on the bubble surface and the potentials ϕ_{1c}. Eq.B13 will then provide the cell potential on the Fluid 2 side as $\phi_{2c} = F + \alpha\phi_{1c}$.
4) The system of equations B19 then provides v_{1c}.
5) Through the kinematic condition at the surface $D\underline{x}/Dt = \underline{u}$, the position of all the nodes on the bubble and cell are updated.

The numerical scheme can then proceed with the next time step and the above procedure is repeated.

The current framework can easily be extended to more than two fluids. Note that in Klaseboer and Khoo[18] a typographical error has occurred in Eq.29, in which the term $C_{p,i}+A_4$ on the right hand side of the equation should have been $C_{p,b}+A$ and another one in Klaseboer and Khoo,[19] where the term $\underline{\underline{A'}}_4 \cdot \underline{F}$ should obviously have been $\underline{\underline{A''}}_4 \cdot \underline{F}$ in Eq.36.

References

1 J. R. Blake and D. C. Gibson, *Annu. Rev. Fluid Mech.*, 1987, **19**, 99-123.
2 O. Behrend and H. Schubert, *Ultrason. Sonochem.* 2001, **8**, 271-276.
3 A. Vogel, *Phys. Med. Biol.*, 1997, **42**, 895–912.
4 A. Vogel and V. Venugopalan, *Chem. Rev.*, 2003, **103**, 577–644.
5 Y. A. Pishchalnikov, O. A. Sapozhnikov, M. R. Bailey, J. C. Williams Jr., R. O. Cleveland, T. Colonius, L. A. Crum, A. P. Evan and J. A. McAteer, *J. Endourol*, 2003, **17**, 435–446.
6 S. Zhu, F. H. Cocks, G. M. Preminger and P. Zhong, *Ultrasound in Med & Biol*, 2002, **28**, 661–671.

7 K. Iqbal, S. W. Ohl, B. C. Khoo, J. Neo and A. S. Fawzy, *Ultrasound in Medicine and Biology*, 2013, **39**, 825-833.
8 A. Shrestha, S. W. Fong, B. C. Khoo, A. Kishen, *Journal of Endodontics*, 2009, **35**, 1028-1033.
9 P. Prentice, A. Cuschieri, K. Dholakia, M. Prausnitz and P. Campbell, *Nature Physics*, 2005, **1**, 107-110.
10 E. J. Park, J. Werner and N. B. Smith, *Pharm. Res.*, 2007, **24**, 1396-1401.
11 M. R. Prausnitz and R. Langer, *Nature Biotech.*, 2008, **26**, 1261-1268.
12 K. Ferrara, R. Pollard and M. Borden, *Annu. Rev. Biomed. Eng.*, 2007, **9**, 415-447.
13 P. Marmottant and S. Hilgenfeldt, *Nature*, 2003, **423**, 153-156.
14 R. Dijkink, S. Le Gac, E. Nijhuis, A. van den Berg, I. Vermes, A. Poot and C. D. Ohl, *Phys. Med. Biol.*, 2007, **53**, 375-390.
15 T. Tandiono, D. S. W. Ow, L. Driessen, C. S. H. Chin, E. Klaseboer, A. B. H. Choo, S. W. Ohl and C. D. Ohl, *Lab Chip*, 2012, **12**, 780-786.
16 Q. X. Wang, K. S. Yeo, B. C. Khoo and K. Y. Lam, *Theor. Comput. Fluid Dyn.*, 1996A, **8**, 73-88.
17 Q. X. Wang, K. S. Yeo, B. C. Khoo and K. Y. Lam, *Comput. Fluids*, 1996B, **25**, 607-628.
18 E. Klaseboer and B. C. Khoo, *J. Appl. Phys.*, 2004, **96**, 5808-1818.
19 E. Klaseboer and B. C. Khoo, *Computational Mechanics*, 2004, **33**, 129-138.
20 P. A. Quinto-Su, C. Kuss, P. R. Preiser and C. D. Ohl, *Lab chip*, 2011, **11**, 672-678.
21 H. Lamb, *Hydrodynamics*, Dover Publications, New York, 1932.
22 L. Rayleigh, *Phil. Mag.*, 1917, **34**, 94–98.
23 C. E. Brennen, *Cavitation and Bubble Dynamics*, Oxford University Press, 1995.
24 M. J. Colbert, A. N. Raegen, C. Fradin and K. Dalnoki-Veress, *Eur. Phys. J. E*, 2009, **30**, 117-121.
25 H. Chen, W. Kreider, A. A. Brayman, M. R. Bailey and T. J. Matula, *Phys. Rev. Lett.*, 2011, **106**, 034301.
26 A. A. Becker, *The boundary element method in engineering, a complete course*, McGraw-Hill Book Company, 1992.
27 P. V. Zinin and J. S. Allen III, *Phys. Rev. E*, 2009, **79**, 021910.
28 A. K. Chesters, *J. Fluid Mech.*, 1977, **81**, 609-624.